

RESEARCH

Open Access



60 GHz RF module with beam-steering optimization algorithm for high data rate access and backhaul communications

Imran Aziz^{1,2*} , Björn Franzén³, Erik Öjefors⁴ and Dragos Dancila¹

*Correspondence:
imran.aziz@angstrom.uu.se

¹ Department of Electrical Engineering, Uppsala University, 751 03 Uppsala, Sweden

² Department of Electrical Engineering, Mirpur University of Science and Technology (MUST), Mirpur, AJK 10250, Pakistan

³ SiversIMA, 421 31 Gothenburg, Sweden

⁴ SiversIMA, 164 40 Kista, Sweden

Abstract

This paper presents an 802.11ad-based radio frequency module for high data rate fixed wireless access and backhaul communications. The transceiver chip is manufactured in SiGe BiCMOS technology covering 57–71 GHz, providing 16 RX and 16 TX paths with combined output power of more than 20 dBm. The chip is packaged using embedded wafer-level BGA technology of the size $12.6 \times 12.6 \times 0.8$ mm³ and employs advanced dielectric materials with 2 metallic redistribution layers. The package integrates the transceiver chip with RX and TX high gain PCB antenna arrays, allowing effective isotropic radiated power (EIRP) of more than 40 dBm. Beam steering is achieved in $\pm 50^\circ$ by the transceiver through providing appropriate weights to the antenna arrays. The paper presents generation of beamforming lookup table along with optimization of the power distribution to the array. This optimization results in flattening of the EIRP over the whole beam-steering range and frequency bandwidth. The module allows for data rates up to 10 Gbps by employing full-channel 128 QAM and half-channel 256 QAM single-carrier modulation.

Keywords: WiGig, 60 GHz transceiver, Beam steering

1 Introduction

Millimeter-wave (mm-wave) 5G networks have great potential and are needed to increase data transfer beyond the existing LTE and sub-6 GHz networks. Technology is developed for both indoor (e.g., multimedia streaming, virtual reality, gaming, wireless docking, etc.) and outdoor applications (e.g., backhaul and fixed wireless access (FWA), etc.). FWA can be used for gigabit-to-the-home (GTTH) without the need for optical fiber for the last kilometer links. In addition, mm-wave FWA can be employed together with mm-wave backhaul for a complete over-the-air solution, implemented even deeper into the core network. The beam-steering capability of the transceivers is key element in allowing for multipoint-to-multipoint connectivity, thus lowering the operational and infrastructure cost. However, the unlicensed mm-wave band 57–66 GHz comes with the challenge of high oxygen absorption on top of higher atmospheric losses compared to sub-6 GHz, but this can also be seen as advantage when it comes to spatial frequency reuse.

In the state of the art, a transceiver with a single-antenna structure is presented in [1], while [2–5] show transceivers with beam-steering capability. These designs, however, focus mainly on short range, and high data rate indoor applications. The solution presented in [6] targets outdoor applications but utilizes a complex 1:12 master/slave infrastructure with 144 antenna elements to attain an effective isotropic radiated power (EIRP) of 51 dBm. Furthermore, [7] presents only a transmitter feeding 256 antenna elements to get 45 dBm EIRP.

This paper presents an antenna module based on a 57–71 GHz transceiver chip [8] packaged using enhanced wafer-level ball grid array (eWLB). The package technology provides more pin count compared to wafer-level chip-scale package (WLCSP) with improved electrical performance because of less parasitic electrical interference [9]. The chip deploys 16 RX and 16 TX paths, which are connected to 2×16 PCB antenna arrays [10]. The antenna array is designed using a multilayered PCB structure, where top and bottom patches are electromagnetically coupled to achieve a broadband response. The high gain of the planar antenna array allows to obtain an EIRP of more than 40 dBm in the 57–66 GHz frequency band along with beam-steering capabilities in the range $\pm 50^\circ$. Furthermore, optimization of the power distribution on the antenna array is presented in detail, which results in a flattening of the EIRP over the whole beam-steering range and frequency bandwidth.

The paper is further organized as follows: sect. 2 of the paper presents the beamforming front-end of the transceiver, with emphasis on the phase shifters, while sect. 3 discusses the technique used to generate the beam-steering lookup table where each entry decides a specific beam angle. An overview of the performance of the eWLB package is provided in sect. 4, while sect. 5 briefly presents the PCB antenna array and transceiver integration. Section 6 presents the optimized beam-book characteristics and antenna array radiation pattern along with over-the-air measurements using different channel bandwidths and modulation schemes. A table comparing the state-of-the-art work is presented in the concluding sect. 7.

2 Transceiver beamforming

The transceiver chip TRX BF/01, operating at 57–71 GHz, consists of 16 RX/16 TX paths as shown in Fig. 1. Independent antenna paths for RX and TX are employed mainly to get around switching losses. Each antenna path can shift the phase and scale the amplitude, by a vector phase shifter. In addition, the transmitter has 26 dBm aggregated saturated power, a typical receiver noise figure of 7 dB, while both RX and TX have 32 dB of dynamic gain range. A zero-intermediate frequency (IF) architecture is used in the transceiver design together with an integrated LO generated at 1/3rd the final frequency.

2.1 Phase shifters

For beamforming purposes, each antenna path has a 6-bit vector phase shifter associated with it. To gain an intuitive understanding of its operation, consider the block-level illustration of a single-receiver path given in Fig. 2. For the simplest case, assume that a single sinusoid is applied to the input of the phase shifter. Following the input, the signal is split in two paths, where one path is phase delayed by 90° . Each path is then injected into gilbert-cell-type mixers which act as ideal amplifiers, capable of both positive and

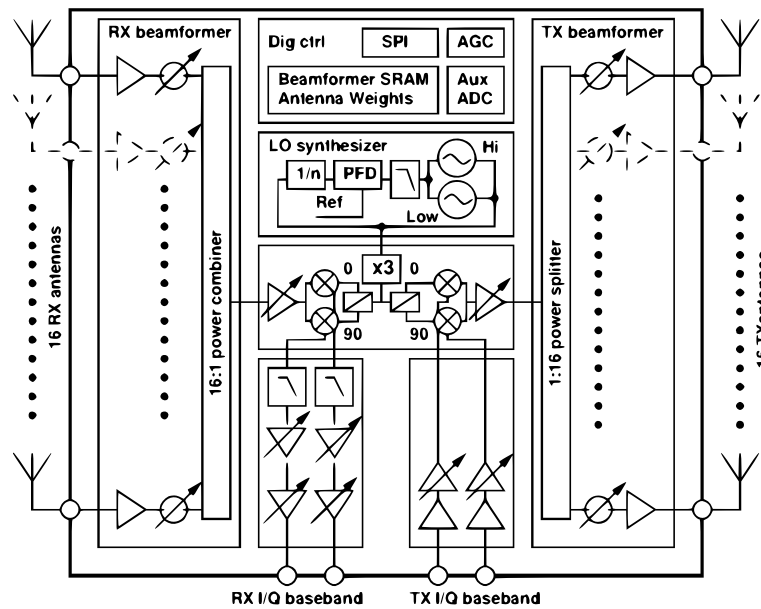


Fig. 1 Block diagram of the 16 TX/16 RX transceiver chip showing the beamforming blocks, up-/down-converter, LO generation, TX/RX baseband, and digital control block

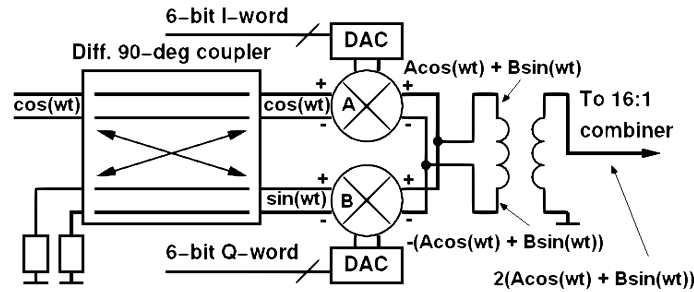


Fig. 2 Block-level representation of a single-receiver beamformer path, highlighting the signal behavior at each cross section of the I-Q phase shifter

negative gain. The two mixer’s differential outputs are tied together to form two summation nodes with opposite polarity. These two nodes are applied to the input to a balun to convert the differential signal to single-ended. Following the annotation in Fig. 2, the phase shifter implements the function given in Eq. 1,

$$\begin{aligned}
 f(t, A, B) &= A \cos(\omega t) + B \sin(\omega t) \\
 &= \sqrt{A^2 + B^2} \cos(\omega t + a \tan 2(-B, A))
 \end{aligned}
 \tag{1}$$

By data fitting experimental data obtained from network analyzer measurements, the ideal relationship can be shown to be approximately valid in the actual implementation as well,

$$f(t, I, Q) = \sqrt{\frac{(I - 31.5)^4 + (Q - 31.5)^4}{231.5^4}} \cos(\omega t + \text{atan2}(Q - 31.5, I - 31.5)) \tag{2}$$

where $I, Q \in \{0, 1, \dots, 62, 63\}$ are the digital control words written to the phase shifter. The phase is normalized such that $(I, Q) = (63, 31)$ is equal to 0° in order to conform with the convention that I is on the real axis in the complex plane, and Q is on the imaginary axis. Furthermore, the unit is voltage, or current, as this is the unit typically used when referring to amplitude tapers.

As can be seen in Fig. 3a and b, the data fit is accurate enough to capture the overall behavior and provide an understanding of the phase shifter, but has insufficient accuracy to use for beamforming purposes. For beamforming purposes, it is necessary to find a set of I, Q values that give constant amplitude, but also represent an unbroken chain of phase values with sufficiently small steps between them. It is clear from

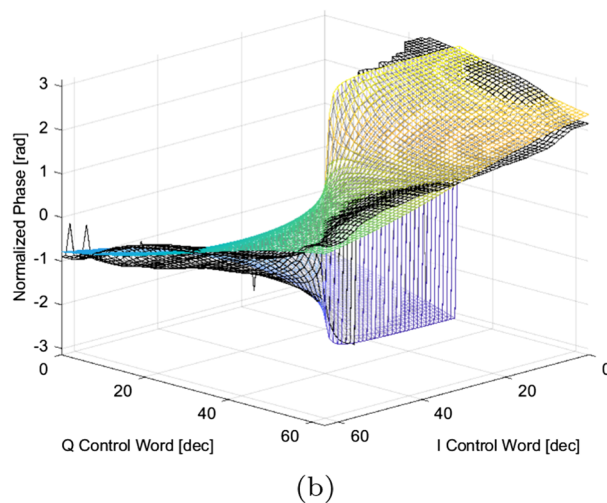
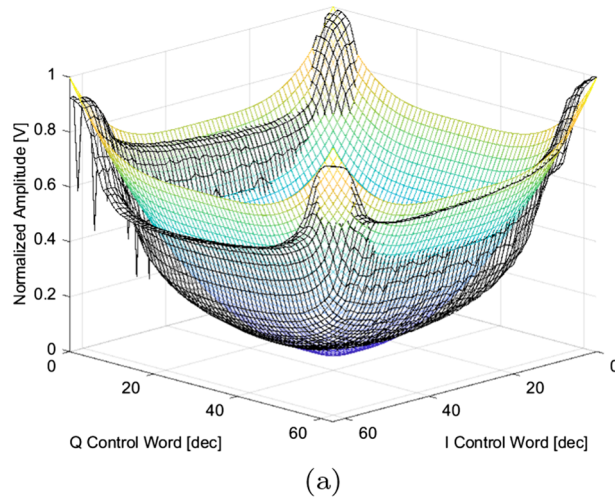


Fig. 3 Amplitude (a) and phase (b) as a function of all control word values. The colored surface is fitted data, and black is the measured data

Fig. 3a that the corner settings, $(I, Q) \in \{(0, 0), (63, 0), (0, 63), (63, 63)\}$, have approximately constant amplitude. Figure 3b, however, shows that the corners are 90° apart in phase, leading to a phase error of up to 45° . It is obvious then, that in order to increase the phase resolution, the amplitude must be decreased from maximum. This is illustrated in Fig. 4 for a few fixed amplitudes.

Figure 4 shows the difference in phase between adjacent phase settings, given that the amplitude is kept close to constant. How much the amplitude can be allowed to vary has to be weighed against the desired phase error, as these are conflicting criteria. Also, note the asymmetry between the corner settings at $\pm 135^\circ$ and 0° . This is due to the gain being slightly different between the I and Q amplifier. This undesired deviation from design forces the amplitude to be backed off an additional 1 dB in order to keep the phase error low. Looking at Fig. 4, it can be seen that if the amplitude is backed off at least 5 dB from maximum, the difference in phase between adjacent settings can be kept lower than 13° , given that the amplitude is allowed to vary ± 0.7 dB. This corresponds to a maximum phase error of 6.5° . For higher amplitudes, the phase error naturally increases. It can then be concluded that in order to produce high-quality array antenna weights, each phase shifter will have at least a 5 dB loss of gain associated with it. However, if low side lobe levels (SLLs) are not a main concern, higher amplitudes can be used.

2.2 Digital control block

The lookup table containing antenna weights/phase shifter control words for each beam is stored in the on-chip 32×1 kbits static RAM (SRAM). Apart from the $2 \times 16 \times 64$ -entry lookup tables, the digital block also contains autonomous automatic gain control (AGC) utilizing RX baseband detectors, a transmitter autonomous level control (ALC) as well as state machines for VCO calibration.

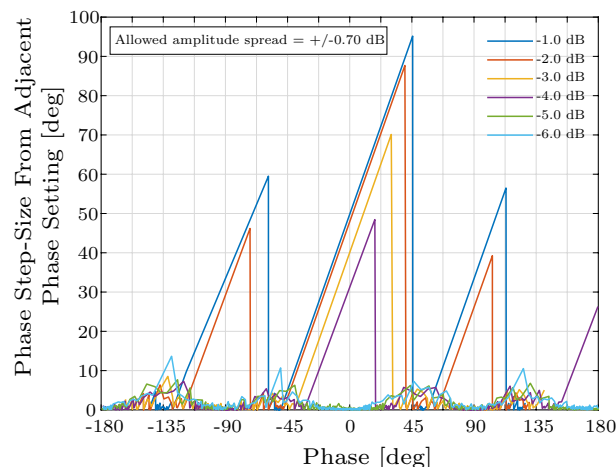


Fig. 4 Phase step size between adjacent phase settings at 58.32 GHz, for a number of fixed amplitudes. 0 dB is set to the highest possible amplitude

3 Method to generate a beamforming lookup table

To steer the radiated power in different directions, antenna element weights are typically obtained with the help of measurements with a network analyzer. The relationship between amplitude/phase and phase shifter control word is then measured by a network analyzer for each antenna path. As each antenna path is thus fully characterized, the element weights can be derived from well-established theory. A drawback to this method is the cost of the network analyzer. For this reason, the method described here instead uses a considerably cheaper power meter together with a brute-force method of finding the phase shifter control words which yields the highest radiated power.

Figure 5 shows the measurement setup used to generate the beamforming lookup table, subsequently referred to as the beam-book, for the transmitter. The antenna module is fixed to a turntable, and a quadrature signal is applied to the baseband inputs. The baseband signal is a sinusoid with fixed amplitude and frequency, which at the antenna ports becomes offset by the LO frequency and scaled in amplitude. To receive the signal from the antenna module, a horn antenna with 20 dB gain is placed at distance of 2 m, angled toward the antenna module. The horn antenna is connected to a power meter, and both the antenna module and the receiving horn antenna are enclosed within an anechoic chamber.

When generating the beam-book for the receiver, the procedure is similar. The main difference being that the horn antenna is instead fed by a signal generator and the power meter is attached to the baseband output. The algorithm used to form the beam-book can in its simplest form be broken down into the following steps:

- 1 Align the turntable to X degrees, $X = \{-50, \dots, 50\}$.
- 2 Set the phase shifters to $0 \times 1F1F$ in all antenna paths. No antenna element is then radiating power, but each antenna element remains correctly impedance matched.
- 3 Set the phase shifter in the 8th antenna path (RF 8) to a fixed value. Here, 0×0000 has been used. The value must be fixed over all beams as the automatic level control (ALC) measures the power at the last stage in the signal chain. A varying value over beams would cause the controlled power to be inconsistent over beams.
- 4 For the 7th antenna path (RF 7), sweep a set of constant amplitude phase shifter values. For each value, measure the power received by the horn antenna.
- 5 Set the phase shifter in the 7th antenna path to the setting with the highest transmitted power and save this value.

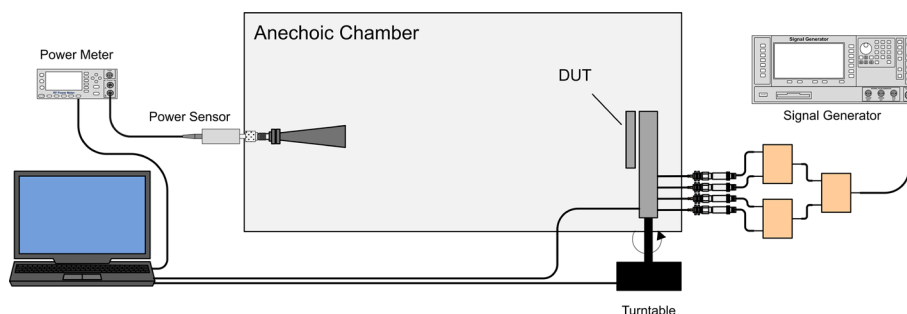


Fig. 5 Illustration of the measurement setup used to generate the Tx side beamforming lookup table

- 6 Repeat steps 4–5 for RF 9, then RF 6, then RF 10, and continue in this fashion to work outward from the center elements to the edge elements.
- 7 When all elements have been optimized, and the array is fully aligned in power, repeat 4–6 to see if some elements can be better optimized now that the entire array is activated.
- 8 Repeat steps 1 through 7 for a new turntable angle until all angles have been measured.

In a low cost application, it is desirable to avoid factory calibration of each antenna module. As such, it is desirable to generate a single beam-book which can be used for all modules. Because of manufacturing spread between units, a given beam-book will have slightly different behavior on each unit. A way to combat this problem is to generate a beam-book on at least two units and then measure the radiation patterns of all beam-books, on a set of units. The beams that satisfy a given criteria for all units can then be selected and saved to a new beam-book. A suitable criterion is a given side lobe level (SLL). We thus add the following steps:

- a) Repeat steps 1 through 8 for N units, $N \geq 1$.
- b) Measure the radiation pattern of each N beam-books on M units. Preferably set $M \geq 5$.
- c) Compare the SLL of each beam, for each beam-book and unit. Let each beam, in each beam-book, be represented by the unit which showed the worst SLL. Then, for each beam, choose the beam-book with the best SLL that is above a given criteria. If no beam-book suits the criteria, increase N and repeat (a) through (c).

There is an additional improvement to the algorithm that must be made that is related to the TRX BF/01 itself. The transmitter suffer from insufficient gain to fully saturate the signal chain at high junction temperatures and at the end of the frequency band. A consequence of this is that low-level modulation schemes, such as QPSK, which can operate close to saturation, cannot be utilized fully if the phase shifters lowers the gain in the signal chain. Ideally, then, the corner settings of the phase shifter should be used. As these settings suffer from poor phase resolution, a trade-off between SLL and EIRP has to be made. The adopted strategy is to increase the phase resolution of the edge elements and, as a consequence, decrease their amplitude, but let as many center elements as possible have high amplitude, but low phase resolution. To optimize that ratio between amplitude and phase resolution, one way is to generate additional beam-books, each with increasing levels of amplitude tapering. Step 5 is thus modified to allow for different elements having different amplitudes. It should also be noted that the array elements are not normalized in amplitude for the same reason, to not lower the available gain. For modest side lobe criteria, this is un-problematic.

By measuring additional beam-books with different amplitude tapers, which infers varying radiated power, it is also possible to flatten the amplitude envelope over steering angles. This is desirable if it can be done with little loss in maximum output power, as it ensures that the same power is transmitted in all directions. It thus simplifies, and improves, output-level control as the on-chip ALC cannot regulate

power variation over beams because it only senses the power in one antenna path. To accommodate multiple amplitude tapers, steps 1–8 should be redone for each taper, and step c should be replaced by

- iii) Compare the SLL of each beam, for each beam-book and unit. Let each beam, in each beam-book, be represented by the unit which showed the worst SLL. The result is an $N \times K$ matrix, N being the number of units the beam-books has been generated on, and K the number of different amplitude tapers that was used. Remove the indices with SLL less than a given criteria and sort the list with the worst SLL first. The sorting order follows from the fact that the worst SLL will correspond to the highest main lobe power.
- iv) Pick the first index where the main lobe power is below a given criterion, e.g., -1 dB from peak power. Write the phase shifter setting corresponding to this value to the new beam-book.

So far, it has not been touched upon how the phase–amplitude relation of the phase shifters should be obtained. If data from network measurements are unavailable, the output power resulting from each phase shifter setting can instead be measured with the same setup as in Fig. 5, with the module aligned directly facing the horn antenna. The procedure is then to measure the radiated power for each control word combination, for each antenna path, and with the bias currents in all other antenna paths turned off in order to avoid interference from other elements. To approximate the phase, Eq. 2 can be used. This method has been used in all measurements.

An example of how the algorithm performs is illustrated in Figs. 6 and 7 for a different type but similar antenna module [11]. Here, $N = 2$, $M = 5$, and $K = 10$. The algorithm can pick from the K amplitude tapers shown in Fig. 7. The SLL criteria are set to ≤ -10 dB, and Fig. 6a shows that this criterion has been mostly fulfilled for the $M = 5$ units it was measured on. A certain flattening of the amplitude envelope was also chosen. Without it, there would be sharp power drops at certain beams where the SLL was high enough that strong tapering was necessary. Figure 6b shows a comparison of the envelope between no tapering (highest possible power, high SLL) and tapering only to reduce SLL (sharp power drops at certain beams, but the high overall envelope), and reduced SLL together with flattened power (better ALC control, medium power and low SLL).

4 Technology and packaging

The transceiver chip used in this work has been packaged using the eWLB packaging solution. This solution outperforms the traditional flip-chip or wire-bonding alternatives in a number of ways, for instance, integration with reduced interconnection length, less conductance, and dielectric losses as well as improved design flexibility [12]. Besides, a key factor for this selection over other complex and comparatively expensive solutions is that eWLB is surface mount device (SMD) packaging technology, which simplifies the upstream assembly process.

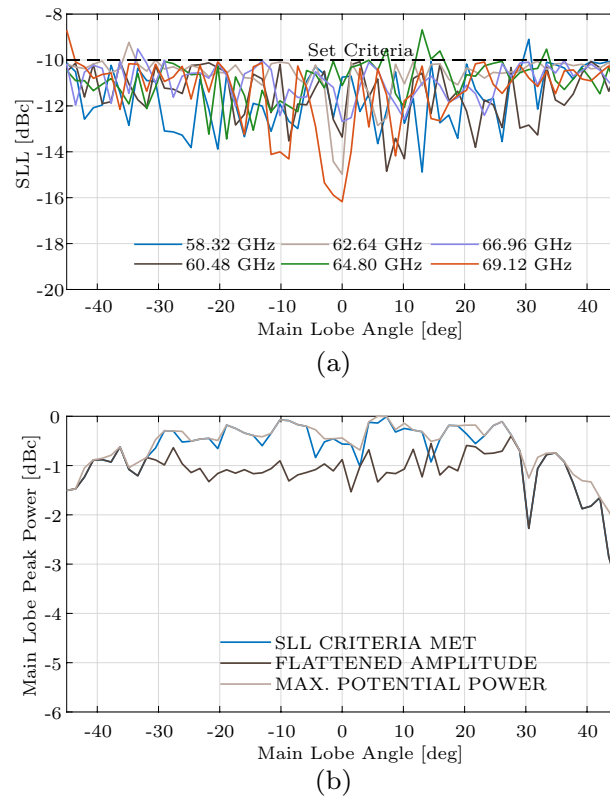


Fig. 6 An example of algorithm performance as measured on a different antenna module type [11] **a** worst case side lobe levels from combined measurements on 5 units, **b** comparison of the amplitude envelope at 58.32 GHz between two beam-books and the potential power of the antenna module, when the phase shifters are set to maximum gain

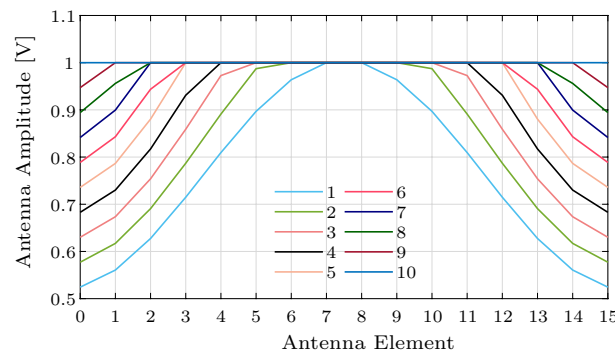


Fig. 7 $K = 10$ chosen amplitude tapers where the sharpest taper is based on a Taylor window. The amplitude is normalized to the phase shifter corner setting with lowest gain

4.1 WiGig eWLB assembly

As shown in Fig. 8a, a two redistribution-layer (RDL) process is used in the package for routing of RF, IF, power, digital control, and baseband signals resulting in a $12.6 \times 12.6 \text{ mm}^2$ large package with 314 solder balls on a 0.5-mm pitch grid. Advanced

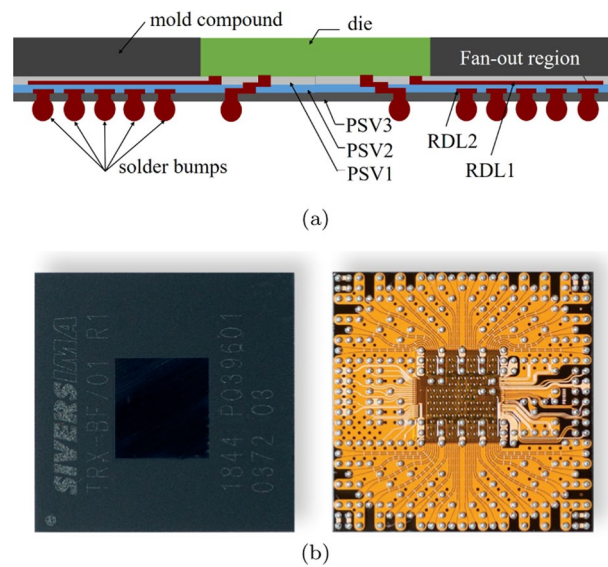


Fig. 8 The eWLB package $12.6 \times 12.6 \times 0.8 \text{ mm}^3$ **a** expanded layout containing 2xRDL, 3xPSV and a single layer of mold compound, **b** Top and bottom of the fabricated packaged chip

dielectric materials (ADMs) with low-temperature curability are used for vigorous reliability of the package [13]. ADMs are a good choice to lessen stress on low thermal budget devices, like thermo-sensitive embedded memory. The requirement of multilayer RDL for design flexibility is higher for system integration, as the device performance is increased with high frequency. Figure 8b shows the fabricated packaged chip where on the left is the top view with black shining chip in the center surrounded by the mold. The right image shows the bottom side of the package where 16 x GSG lines on each upper and lower half will be connected with the PCB antenna arrays through shown solder balls.

4.2 Electrical performance and characterization

The RF signal is directed from the chip pads to CPW lines on RDL, which is connected to microstrip line on the PCB through solder bumps. Figure 9 shows this transition from RDL to PCB, designed using HFSS software. A final confirmatory simulation is performed by importing full package RF layout, containing all paths and interconnects, and the results show a package loss of $\approx 2\text{dB}$ in the frequency band 57 GHz-71 GHz.

The eWLB package performance is validated by comparing the measurements for bare die and packaged die. For a single-antenna path, Fig. 10a, b shows the comparison of compressed output power and noise figure (NF), respectively. The values vary due to different source and load impedances when bare die is probed compared to packaged die. The gap between the two curves in Fig. 10a presents the losses of the package including transition to the PCB.

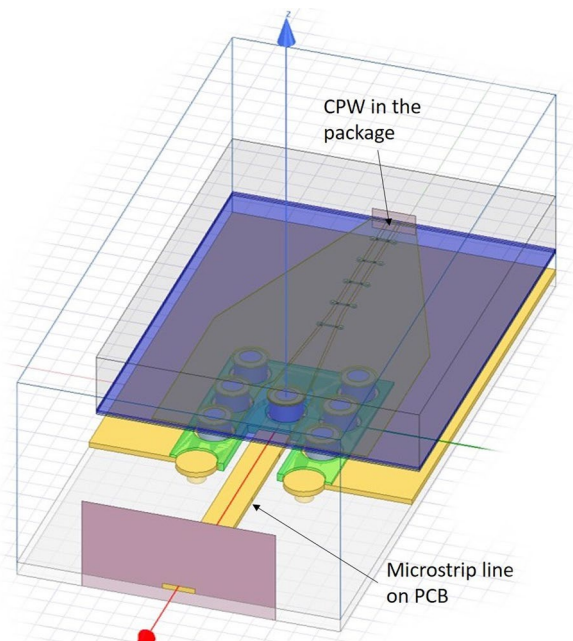


Fig. 9 Subset of the 3D package model including coplanar waveguide (CPW) port, transition from package to PCB, and microstrip on the PCB

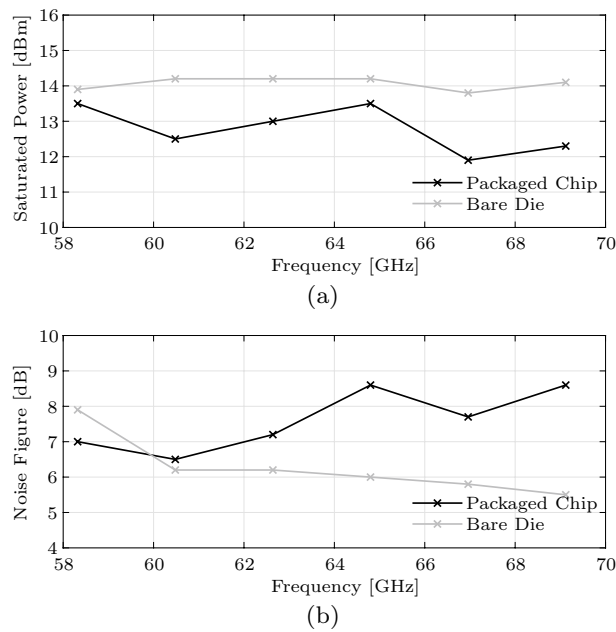


Fig. 10 Single-antenna path bare die vs packaged chip **a** compressed output power **b** noise figure

5 PCB antenna arrays and transceiver integration

As planar antennas have the ease of integration with the RFIC, a multilayer stacked patch antenna is designed to achieve broadband performance [14–17]. The antenna array used in this work is a 2×16 array, where each sub-array is a 2-element series fed

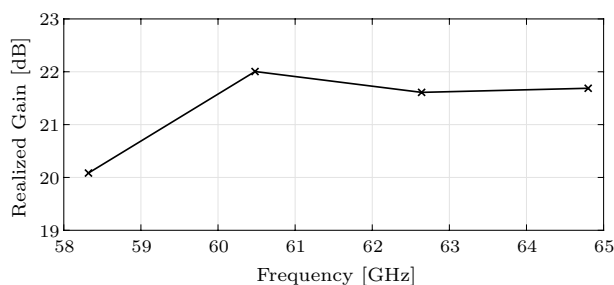


Fig. 11 Maximum realized gain for 2×16 antenna array simulated at center frequencies of 802.11ad channels 1–4

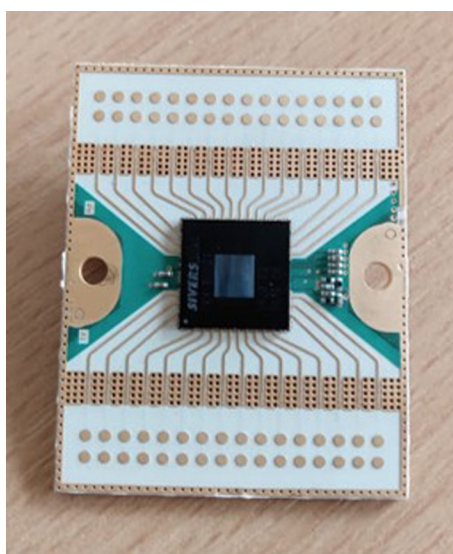


Fig. 12 2×16 PCB antenna arrays integrated with eWLB packaged transceiver. The PCB size is 50×40 mm²

patch array. The circular patches on top metallic layer of the sub-array are electromagnetically coupled with the rectangular patches which are series fed through a microstrip line. The detailed design is presented in Fig. 1d of reference [10]. The maximum realized gain of the antenna array is presented in Fig. 11 for the center frequencies of 802.11ad channels 1–4. The results show more than 20 dBi realized gain for the whole band.

The eWLB packaged transceiver feeds the 2×16 TX and RX arrays separately as shown in Fig. 12. The sub-arrays in the center have shorter microstrip lines than the ones on the edges, for which the phase can be compensated in the transceiver beam-book. Each transceiver path provides a single column of the antenna array with specific amplitude and phase, and the main beam of the antenna array can be steered in the H-plane by providing progressively increasing or decreasing phases. When main beam of the array is steered toward maximum angle θ , the grating lobes can start appearing in the radiation pattern. Equation 2 presents the criteria needed to avoid these grating lobes in terms of spacing d between adjacent sub-arrays [18].

$$d < \frac{\lambda_o}{1 + \sin \theta} \quad (3)$$

which means that for higher beam-steering angles, the element spacing should be reduced. To elaborate, for broadside radiation, i.e., $\theta = 0^\circ$, the equation reduces to $d < \lambda_o$ and for $\theta = 90^\circ$, $d < \lambda_o/2$. As we aim to steer the beam at maximum $\pm 50^\circ$, this spacing should be less than 2.8 mm in order to avoid the grating lobes. However, $d = 2.2$ mm is used in the design to make the solution more compact.

6 Results and discussion: beam-book characteristics and measured array radiation pattern

A comparison between a beam-book using solely the phase shifter's corner settings (maximum power) and a beam-book generated with the proposed algorithm ($K = 10$, $N = 1$, $M = 1$, $SLL < -9$ dBc, flattened amplitude) is shown in Fig. 13. The measurement is performed at 85 °C junction temperature, the maximum temperature the transceiver is specified for. It is clear that corner settings work fairly well despite their $\pm 45^\circ$ phase error. Looking at Fig. 13a, b, the corner settings beam-book can deliver 44–43 dBm EIRP at CH 1–3 with a 3 dB bandwidth covering all angles. An outlier is CH 4, showing only 41 dBm maximum output power, but its amplitude envelope is essentially flat. Because it is desired that the envelope is flat, and this would normally be achieved by tapering, the effective power is similar between channels. The proposed algorithm results in 1 dB lesser EIRP with the same bandwidth, but flatter amplitude envelope. It shows that only minimal tapering is required to sufficiently flatten the envelope and bring the SLL down to the desired level. It should, however, be emphasized that the SLL criterion is application based and if 9 dBc suppression is insufficient, the loss in maximum EIRP will be higher.

Another observation, which follows intuitively from the higher phase error of the corner settings beam-book, is the lower angular accuracy in where the main lobe is at maximum power. It can clearly be seen in Fig. 13f that the center beams with high tapering have considerable better accuracy. Moreover, comparison of Fig. 13g, h shows that the beamwidth increases with higher tapering. This is expected as the power that is removed from the side lobes is instead shifted to the main lobe.

Figure 14 shows the radiation patterns for the beam-book which uses the corner settings. It shows that there are no grating lobes present and that the envelope of the individual beams are well behaved, with the possible exception of one of the edge beams at 60.48 GHz. As the outlying behavior of this beam is not present with other amplitude tapers, it might be a result of phase shifters settings and not related to the antenna array itself.

6.1 Over-the-air measurements

The evaluation kit, shown in Fig. 15, is a platform designed for evaluation of the presented WiGig module (transceiver RFIC integrated with PCB antenna array) [11]. The kit contains an IDT modem IC RWM6050 but can also be operated with other baseband solutions. A metallic heatsink with thermal interface material is used on top of the chip for

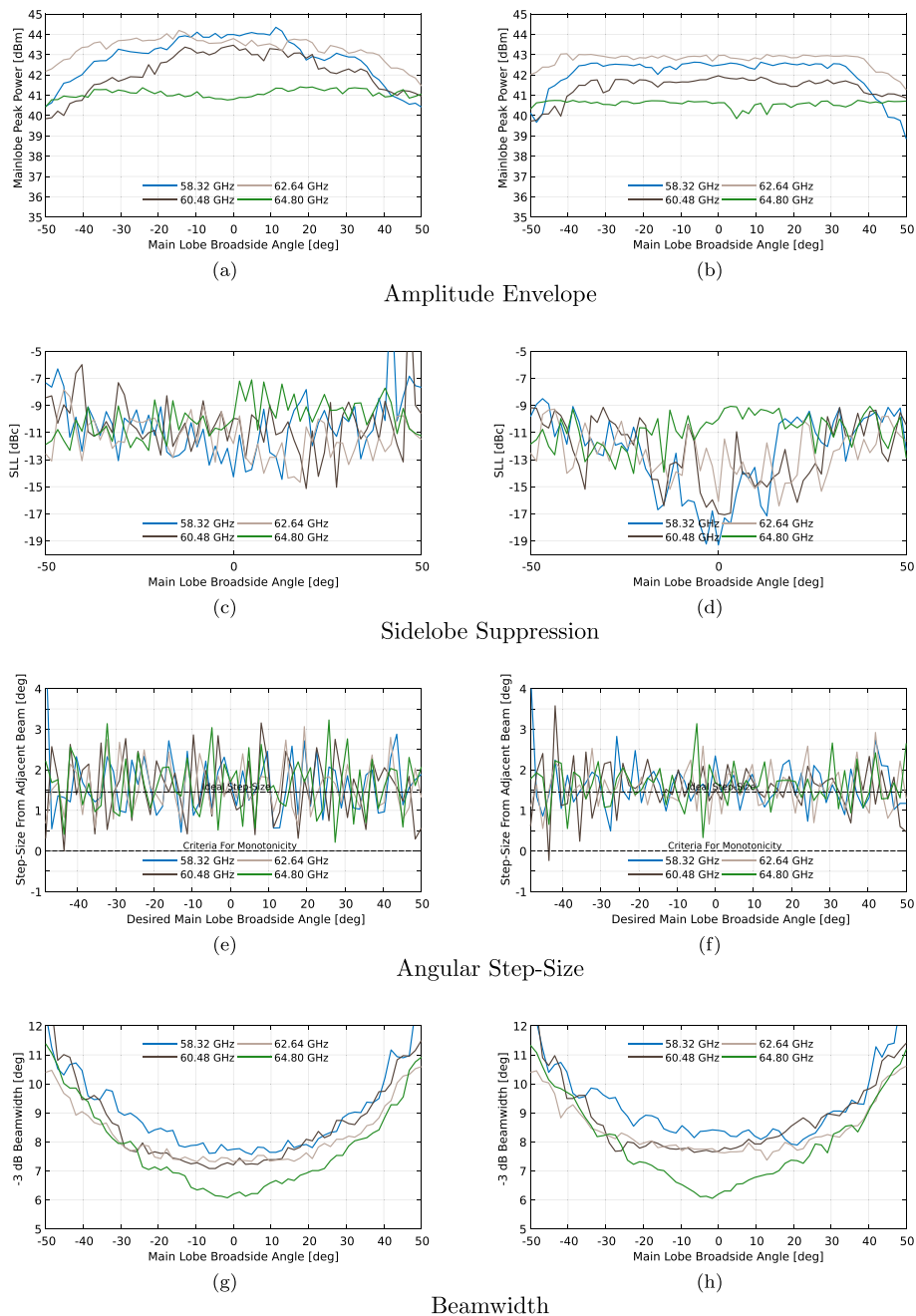


Fig. 13 Comparison of two beam-books; (left) phase shifters set to corner settings (maximum power), (right) generated with the proposed algorithm ($K = 10, N = 1, M = 1, SLL < -9$ dBc, flattened amplitude). The signal chain is saturated. **a** Mainlobe peak power when phase shifters are set to corner settings. **b** Mainlobe peak power when phase shifters are set using the proposed algorithm. **c** SLL when phase shifters are set to corner settings. **d** SLL when phase shifters are set using the proposed algorithm. **e** Step size with adjacent beam when phase shifters are set to corner settings. **f** Step size with adjacent beam when phase shifters are set using the proposed algorithm. **g** -3 dB beamwidth when phase shifters are set to corner settings. **h** -3 dB beamwidth when phase shifters are set using the proposed algorithm

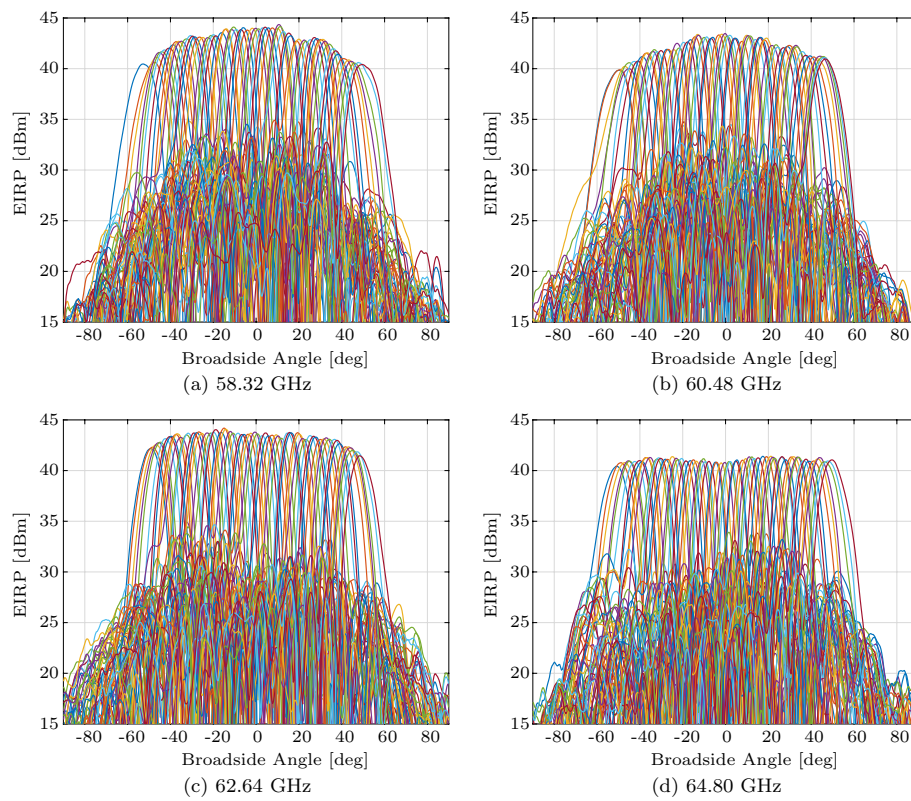


Fig. 14 Radiation pattern of the four WiGig channels covered by the antenna module. The phase shifters are set to maximum gain and the signal chain is saturated

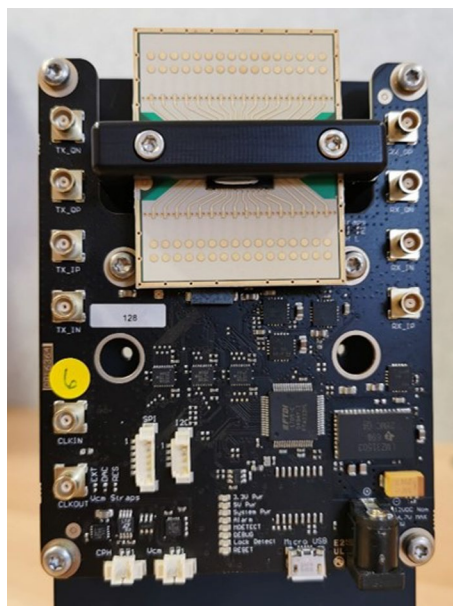


Fig. 15 60 GHz WiGig evaluation kit for 802.11ad beam-steering transceiver RFIC integrated with 2x16 antenna array. A metallic heatsink is placed on top of the chip for efficient heat transfer

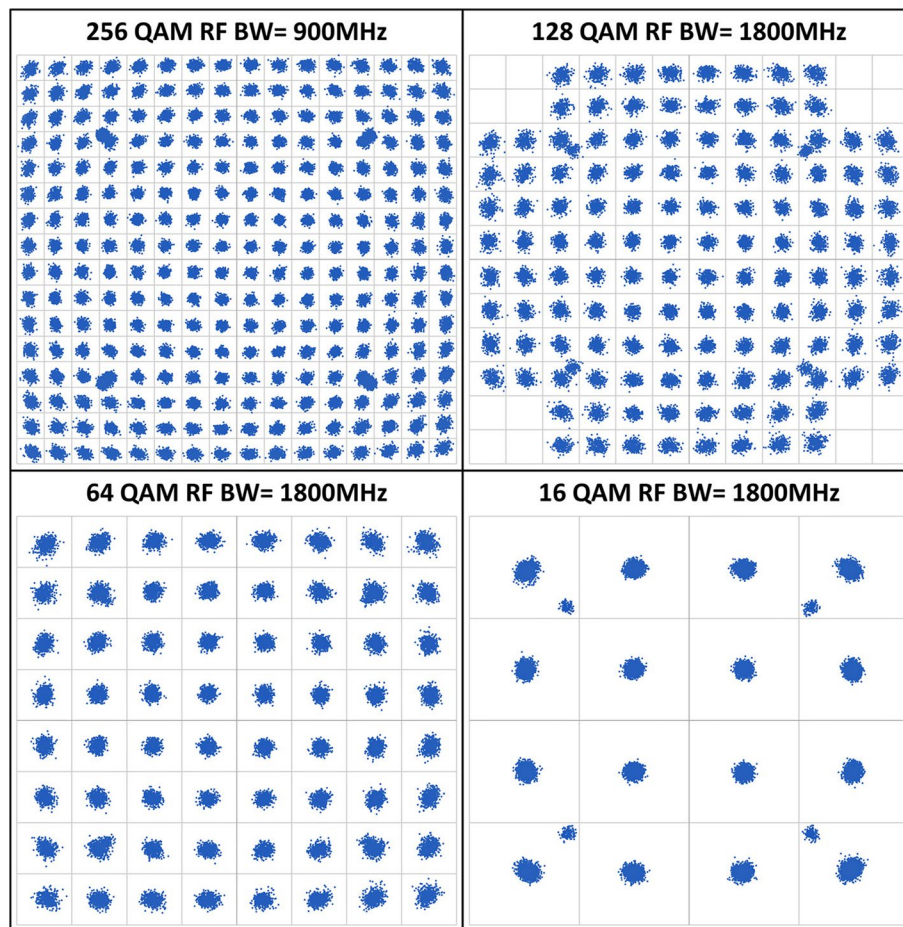


Fig. 16 Measured single-carrier QAM constellations with an over-the-air TX-to-RX link when beams are steered at 45° from the broadside

efficient heat transfer. Figure 16 shows the constellation diagrams of over-the-air TX–RX link measurements for different channel bandwidths and QAM modulations. The diagrams present wireless communication up to 10 Gbps using full channel bandwidth of 1.8 GHz with single-carrier 128-QAM modulation, as well as half bandwidth (900 MHz) by employing 256-QAM. For 802.11ad standard modems, only up to 16 QAM modulation is supported in single-carrier mode, so a custom modem is employed for the mentioned measurements. The shown measurements are carried out with the TX and RX antenna arrays steered at 45° from the broadside in the azimuth plane.

7 Conclusion

This paper presents a wide-angle beam-steerable 60 GHz WiGig module for access and backhaul wireless systems. The 16 RX/16 TX channels transceiver chip is packaged using eWLB which shows around 2 dB package loss. The chip is integrated with 2×16 antenna arrays which show the realized gain of more than 20 dBi. A comparison of our work with state of the art is presented in Table 1. EIRP of 51 dBm is achieved in [6]; however, it utilizes a complex 1:12 master/slave chip structure with 144-element antenna array.

Table 1 Performance comparison with state-of-the-art solutions

Technology	Ant. elements [circ. blocks]	Oper. freq. [GHz]	Output power [dBm]	HPBW [°]	Max. SLL [dB]	Beam- steering	References
65 nm CMOS digital	32 RX/8 TX	59.4–63.72	28 (EIRP)	Not specified	–	Yes	[2]
40 nm CMOS LP	16 RX/16 TX	57–66	24 (EIRP)	Not specified	– 7	$\pm 60^\circ$	[3]
28 nm/40 nm CMOS	144 RX/144 TX	57–66	51 (EIRP)	≈ 20	– 10	$\pm 60^\circ$	[6]
90 nm CMOS	32 RX/32 TX	57–62	38 (EIRP)	≈ 18	– 7	$\pm 30^\circ$	[20]
120 nm SiGe BiCMOS	16 RX	58.32–64.8	–	Not specified	–	Yes	[4]
120 nm SiGe BiCMOS	16 TX	51–65	21–25.5 (tot. OP1dB)	Not specified	– 5	$\pm 45^\circ$	[5]
130 nm SiGe BiCMOS	1 RX/1 TX	57–66	13.4–16.2 (OP1dB)	Not specified	–	–	[1]
130 nm SiGe BiCMOS	256 TX	58–64	45 (EIRP)	6	– 9	$\pm 55^\circ$	[7]
180 nm SiGe BiCMOS	2x256 TRX	60–64	44 (EIRP)	6	– 8	$\pm 50^\circ$	[19]
180 nm SiGe BiCMOS	2x64 TRX	60–64	38 (EIRP)	12	– 11	$\pm 50^\circ$	[19]
130 nm SiGe BiCMOS	32 RX/32 TX	57–66	44 (EIRP)	7	– 9	$\pm 50^\circ$	This work

Besides, a dual polarized design utilizes 256 elements for each polarization to achieve 44 dBm EIRP [19] in the band 60–64 GHz. The comparison shows that our work outperforms different state-of-the-art work in different aspects and it can be observed that the proposed module is a good candidate when targeting around 40 dBm EIRP and $\pm 50^\circ$ beam steering. Besides, the module has demonstrated up to 10 Gbps data rate using full channel 128-QAM.

Abbreviations

RF:	Radio frequency
FWA:	Fixed wireless access,
eWLB:	Embedded wafer-level ball grid array
RDL:	Redistribution layer
EIRP:	Effective isotropic radiated power
QAM:	Quadrature amplitude modulation
LTE:	Long-term evolution
GTTH:	Gigabit to the home
WLSCP:	Wafer-level chip-scale packaging
PCB:	Printed circuit board
IF:	Intermediate frequency
RAM:	Random access memory
AGC:	Automatic gain control
ALC:	Autonomous level control
VCO:	Voltage controlled oscillator
LO:	Local oscillator
SLL:	Side lobe level
TRX:	Transceiver
QPSK:	Quadrature phase shift keying
SMD:	Surface mount device
ADM:	Advanced dielectric material
GSG:	Ground signal ground
CPW:	Coplanar waveguide
HFSS:	High-frequency structure simulator
NF:	Noise figure
RX:	Receiver
TX:	Transmitter
RFIC:	Radio frequency integrated chip

Acknowledgements

This work has been funded by the Swedish agency, Vinnova, for 60 GHz RF beam-steering solution with phased array antenna for small cell backhaul and wireless access points (Project No: 2016-01800). We acknowledge Mirpur University of Science and Technology (MUST), Pakistan, for financial support of Imran Aziz.

Author contributions

IA has been involved with designing of antenna array, carrying out simulations, and writing of this paper. BF has performed beam-steering optimization and carried out the respective measurements. EÖ and DD have been involved with overall supervision of this work. All authors read and approved the final manuscript.

Funding

Open access funding provided by Uppsala University. Funding was provided by Vinnova Project No: 2016-01800

Declarations

Competing interests

The authors declare that they have no competing interests.

Received: 16 November 2020 Accepted: 6 September 2022

Published online: 24 September 2022

References

1. A. Tomkins, A. Poon, E. Juntunen, A. El-Gabaly, G. Temkine, Y. To, C. Farnsworth, A. Tabibiazar, M. Fakharzadeh, S. Jafarloo, A. Abdellatif, H. Tawfik, B. Lynch, M. Tazlauanu, R. Glibbery, A 60 ghz, 802.11ad/wigig-compliant transceiver for infrastructure and mobile applications in 130 nm sige bicmos. *IEEE J. Solid State Circ.* **50**(10), 2239–2255 (2015). <https://doi.org/10.1109/JSSC.2015.2436900>
2. S. Emami, R.F. Wiser, E. Ali, M.G. Forbes, M.Q. Gordon, X. Guan, S. Lo, P.T. McElwee, J. Parker, J.R. Tani, J.M. Gilbert, C.H. Doan, A 60ghz cmos phased-array transceiver pair for multi-gb/s wireless communications. In: 2011 IEEE International Solid-State Circuits Conference, pp. 164–166 (2011). <https://doi.org/10.1109/ISSCC.2011.5746265>
3. M. Boers, B. Afshar, I. Vassiliou, S. Sarkar, S.T. Nicolson, E. Adabi, B.G. Perumana, T. Chalvatzis, S. Kavvadias, P. Sen, W.L. Chan, A.H. Yu, A. Parsa, M. Nariman, S. Yoon, A.G. Besoli, C.A. Kyriazidou, G. Zochios, J.A. Castaneda, T. Sowlati, M. Rofougaran, A. Rofougaran, A 16tx/16rx 60 ghz 802.11ad chipset with single coaxial interface and polarization diversity. *IEEE Journal of Solid-State Circuits* **49**(12): 3031–3045 (2014). <https://doi.org/10.1109/JSSC.2014.2356462>
4. A. Natarajan, S.K. Reynolds, M. Tsai, S.T. Nicolson, J.C. Zhan, D.G. Kam, D. Liu, Y.O. Huang, A. Valdes-Garcia, B.A. Floyd, A fully-integrated 16-element phased-array receiver in sige bicmos for 60-ghz communications. *IEEE J. Solid State Circ.* **46**(5), 1059–1075 (2011). <https://doi.org/10.1109/JSSC.2011.2118110>
5. A. Valdes-Garcia, S.T. Nicolson, J. Lai, A. Natarajan, P. Chen, S.K. Reynolds, J.C. Zhan, D.G. Kam, D. Liu, B. Floyd, A fully integrated 16-element phased-array transmitter in sige bicmos for 60-ghz communications. *IEEE J. Solid State Circ.* **45**(12), 2757–2773 (2010). <https://doi.org/10.1109/JSSC.2010.2074951>
6. T. Sowlati, S. Sarkar, B. Perumana, W.L. Chan, B. Afshar, M. Boers, D. Shin, T. Mercer, W. Chen, A.P. Toda, A.G. Besoli, S. Yoon, S. Kyriazidou, P. Yang, V. Aggarwal, N. Vakilian, D. Rozenblit, M. Kahrizi, J. Zhang, A. Wang, P. Sen, D. Murphy, M. Mikhemar, A. Sajjadi, A. Mehrabani, B. Ibrahim, B. Pan, K. Juan, S. Xu, C. Guan, G. Geshvindman, K. Low, N. Kocaman, H. Eberhart, K. Kimura, I. Elgorriaga, V. Roussel, H. Xie, L. Shi, V. Kodavati, A 60ghz 144-element phased-array transceiver with 51dbm maximum eirp and ± 60 beam steering for backhaul application. In: 2018 IEEE International Solid - State Circuits Conference - (ISSCC), pp. 66–68 (2018). <https://doi.org/10.1109/ISSCC.2018.8310186>
7. S. Zahir, O.D. Gurbuz, A. Kar-Roy, S. Raman, G.M. Rebeiz, 60-ghz 64- and 256-elements wafer-scale phased-array transmitters using full-reticle and subreticle stitching techniques. *IEEE Trans. Microw. Theory Tech.* **64**(12), 4701–4719 (2016). <https://doi.org/10.1109/TMTT.2016.2623948>
8. E. Öjefors, M. Andreasson, T. Kjellberg, H. Berg, L. Aspemyr, R. Nilsson, K. Brink, R. Dahlbäck, D. Wu, K. Sjögren, M. Carlsson, A 57-71 ghz beamforming sige transceiver for 802.11 ad-based fixed wireless access. In: 2018 IEEE Radio Frequency Integrated Circuits Symposium (RFIC), pp. 276–279 (2018). <https://doi.org/10.1109/RFIC.2018.8428976>
9. M. Wojnowski, M. Engl, B. Dehlink, G. Sommer, M. Brunnbauer, K. Pressel, R. Weigel, A 77 ghz sige mixer in an embedded wafer level bga package. In: 2008 58th Electronic Components and Technology Conference, pp. 290–296 (2008)
10. I. Aziz, R. Dahlbäck, E. Öjefors, K. Sjögren, A. Rydberg, D. Dancila, 60ghz compact broadband antenna arrays with wide-angle beam steering. *J. Eng.* **2019**(8), 5407–5414 (2019). <https://doi.org/10.1049/joe.2018.5343>
11. RF module evaluation kit. <https://www.siversima.com/product/evk-600200/>
12. D. Wu, R. Dahlbäck, E. Öjefors, M. Carlsson, F.C.P. Lim, Y.K. Lim, A.K. Oo, W.K. Choi, S.W. Yoon, Advanced wafer level pkg solutions for 60ghz wigig (802.11ad) telecom infrastructure. In: 2019 IEEE 69th Electronic Components and Technology Conference (ECTC), pp. 968–971 (2019). <https://doi.org/10.1109/ECTC.2019.00151>
13. S.W. Yoon, Robust reliability performance of large size ewlb (fan-out wlp). Additional Conferences (Device Packaging, HiTEC, HiTEN, & CICMT) 2013(DPC), 001438–001457 (2013). <https://doi.org/10.4071/2013DPC-wp21>
14. D.M. Pozar, D.H. Schaubert, *Microstrip antennas: the analysis and design of microstrip antennas and arrays*. Wiley-IEEE Press, ??? (1995). <https://ieeexplore.ieee.org/book/5263382>
15. J. James, P. Hall, *Handbook of microstrip antennas*, pp. 1–3 (1989)
16. R. Bancroft, *Microstrip and printed antenna design* (2nd Edition), 2nd editio edn. SciTech Publishing (2009). Chap. 4. <https://app.knovel.com/hotlink/pdf/id:kt008G2RJ1/microstrip-printed-antenna/broadband-microstrip>

17. T. Zhang, L. Li, H. Xia, X. Ma, T.J.C. Cui, A low-cost and high-gain 60-GHz differential phased array antenna in PCB process. *IEEE Trans. Compon. Packag. Manuf. Technol.* **8**(7), 1281–1291 (2018). <https://doi.org/10.1109/TCPMT.2018.2839342>
18. S.J. Orfanidis, *Electromagnetic Waves and Antennas*, pp. 1111–1114. Rutgers University, ??? (pages 1111–1114, 2016). Chap. Antenna Arrays. <http://ecweb1.rutgers.edu/~orfanidi/ewa/>
19. U. Kodak, B. Rupakula, S. Zahir, G.M. Rebeiz, 60-ghz 64- and 256-element dual-polarized dual-beam wafer-scale phased-array transceivers with reticle-to-reticle stitching. *IEEE Trans. Microw. Theory Tech.* **68**(7), 2745–2767 (2020)
20. E. Cohen, M. Ruberto, M. Cohen, O. Degani, S. Ravid, D. Ritter, A cmos bidirectional 32-element phased-array transceiver at 60 ghz with ltcc antenna. *IEEE Trans. Microw. Theory Tech.* **61**(3), 1359–1375 (2013)

Publisher's Note

Springer Nature remains neutral with regard to jurisdictional claims in published maps and institutional affiliations.

Submit your manuscript to a SpringerOpen[®] journal and benefit from:

- ▶ Convenient online submission
- ▶ Rigorous peer review
- ▶ Open access: articles freely available online
- ▶ High visibility within the field
- ▶ Retaining the copyright to your article

Submit your next manuscript at ▶ [springeropen.com](https://www.springeropen.com)
